Photodissociation Quantum Dynamics of the Ar−HF($v = 0$) Cluster

R. Prosmiti and A. García-Vela*

Instituto de Matemáticas y Fısica Fundamental, C.S.I.C., Serrano 123, 28006 Madrid, Spain

Received: March 31, 2003; In Final Form: May 15, 2003

The ultraviolet photodissociation of Ar−HF($v = 0$) is studied by means of wave packet simulations. Photolysis is simulated from two different cluster initial states, namely, the ground and an excited van der Waals (vdW) state, associated with the Ar−H−X and Ar−X−H isomers, respectively. The photolysis dynamics involves mainly direct dissociation of the hydrogen atom, and at most a couple of subsequent collisions of the recoiling H with Ar and F, for the two cluster initial states. The H/Ar collision has a relatively high probability in the case of the initial ground vdW state, while it is much more unlikely for photolysis from the initial excited vdW state. The probability of Ar−F radical products is calculated for several excitation energies along the range of the Ar−HF($v = 0$) absorption spectrum. A negligible probability of these products is found for the two cluster initial states, for all the energies studied. The result is attributed to the large amount of energy available for the Ar−F fragment, at the excitation energies contained in the Ar−HF($v = 0$) absorption spectrum, which diminishes dramatically the Ar−F survival probability. By comparison of the present results with previous ones on Ar−HX (X = Cl, Br) photolysis, some trends on the photodissociation behavior of this family of clusters are discussed.

I. Introduction

The ultraviolet (UV) photolysis of weakly bound hydrogen-bonded clusters such as Rg_n−HX, $(HX)_n$, and Rg_n−H_2Y (X = halogen, Rg = rare gas, Y = O, S) has been the subject of an increasing interest in the past years, both experimentally[1−13] and theoretically.[11,12,14−32] Upon photoexcitation of the chromophore (HX or H_2Y) to a repulsive electronic state, a fast H fragment is ejected, causing cluster fragmentation through different pathways. When hydrogen recoil is hindered by the surrounding atoms or molecules in the cluster, solvation effects typical of condensed matter environments such as the cage effect can be investigated.[1,9−12,14−25,27b] When the cluster size is increased, the condensed matter limit is gradually approached. On the other side, direct, unhindered hydrogen dissociation may leave behind weakly bound radical complexes,[3,4,8,22,27a,28−32] which allow one to probe the open-shell interactions involved.

Theoretical simulations of photodissociation of tetraatomic and larger clusters such as Ar_n −HF,[18,25] Ar_n −HCl,[16,23,24] Ar_n −HBr,[11,12] Xe_n −HI,[14] Ar−H_2O,[19] and $(HCl)_2$[30] were carried out by means of classical and hybrid quantum/classical methods. Quantum mechanical 3D calculations have been restricted to triatomic Rg−HX clusters, in particular Ar−HCl[17,18,22,27] and Ar−HBr.[21,28b,30,31] In these small prototype Rg−HX clusters, it is possible to carry out a more detailed investigation of the photolysis mechanisms that govern the different fragmentation pathways of the cluster. In addition, characterization of the cluster state initially prepared in the excited electronic surface is more precise in Rg−HX complexes than in larger clusters. This allows one to investigate the effect of the cluster initial state (which determines the distribution of intracluster orientations and impact parameters) on the yield of photolysis products, and thus how to exert control on that yield.[28, 29]

Recent quasiclassical[28a] and wave packet[28b] simulations of the Ar−HBr($v = 1$) photolysis dynamics, as well as wave packet studies of the Ar−HBr($v = 0$) photodissociation,[30,31] have shown dramatic differences in the product yield as compared with the Ar−HCl($v = 0$) photolysis.[26,27] Specifically, the yield of Ar−Br radical complexes is much higher than that of Ar−Cl products, for the same excess energy of the parent cluster. This result was partially attributed to the different amounts of energy available for the Ar−Br and Ar−Cl products in the photodissociation process, due to the different H/Br and H/Cl mass ratios.[28,30,31] Sterical effects inherent to the initial states of Ar−HBr and Ar−HCl, which cause a lower probability of a collision between the recoiling hydrogen and the Ar obstacle in the Ar−HBr case, were also suggested to explain the large differences in the radical product yield.[28b]

The differences found between Ar−HCl and Ar−HBr indicate that halogen substitution affects strongly the photolysis behavior in Ar−HX clusters. In this light, the study of other members of the Ar−HX family different than Ar−HCl and Ar−HBr appears very interesting, to elucidate possible trends in the behavior of the photolysis dynamics upon halogen substitution. The aim of the present work is to report on the wave packet photodissociation dynamics of the Ar−HF($v = 0$) precursor cluster. While the UV photolysis of this system has been investigated classically,[18] to the best of our knowledge the current study is the first quantum mechanical one. Photolysis is simulated by starting from two different initial states of Ar−HF($v = 0$), associated with the Ar−H−F and Ar−F−H isomers of the cluster, respectively. In the case of Ar−HBr($v = 1$) photolysis, a strong effect was found in the product yield as a result of starting from one or the other isomeric form, due to the different initial intracluster geometry distributions.[28] Thus, its possible effect in the Ar−HF($v = 0$) photodissociation is investigated here.

The paper is organized as follows. In section II, the system and the dynamical method used are described. In section III, the results are presented and discussed. Some conclusions are given in section IV.

* To whom correspondence should be addressed. E-mail: garciavela@imaff.cfmac.csic.es.

10.1021/jp0303873 CCC: $25.00
Published on Web 06/24/2003

II. Theory

A. Potential-Energy Surfaces and Initial State. Upon UV excitation of HF from its ground electronic state $X^1\Sigma^+$ to the repulsive excited state $A^1\Pi$, the Ar−HF cluster photodissociates. A Franck−Condon transition between the two electronic states is assumed in our model. The system is represented in the (r, R, θ) Jacobian coordinates, where r is the H−F distance, R is the separation between the Ar atom and the HF center-of-mass, and θ is the angle between the vectors **r** and **R** (with $\theta = 0$ corresponding to the collinear configuration Ar−H−F).

The ground-state potential surface is modeled as a sum of an atom−atom potential for the H−F interaction plus a term reproducing the van der Waals (vdW) interaction,

$$V_g(r, R, \theta) = V^g_{H-F}(r) + V_{vdW}(R, \theta) \quad (1)$$

The V^g_{H-F} term is represented by a Morse functional form with parameters $D = 6.11$ eV, $r_e = 0.919$ Å, and $\alpha = 2.25$ Å^{-1}. These parameters were obtained by fitting to a Morse function the ab initio potential for Na−HF[33] when Na and HF are sufficiently separated. The *H*6(4, 3, 2) intermolecular potential of Hutson[34] was used to describe the vdW interaction term.

The excited electronic state potential is represented as a sum of pairwise interactions between the atoms of the system,

$$V_e = V^e_{H-F} + V^e_{H-Ar} + V^e_{Ar-F} \quad (2)$$

The V^e_{H-F} interaction term in the $A^1\Pi$ excited state is obtained by fitting the ab initio calculations of Dunning[35] to the functional form[18]

$$V^e_{H-F}(r) = Ae^{-\beta r} + \frac{C}{r^{12}} \quad (3)$$

with parameters $A = 61.2$ eV, $\beta = 2.38$ Å^{-1}, and $C = 15.70$ meV Å.[12] Empirical potentials have been used for the H−Ar[36] and Ar−F[37] (in the $X1/2$ ground electronic state) interactions.

In the calculation of the initial state of Ar−HF($v = 0$) in the $X^1\Sigma^+$ surface, the HF stretching vibration is separated within the vibrational diabatic approximation,[38] and the cluster wave function is expressed as

$$\Phi_{v=0,n,b}(r, R, \theta) = \chi_{v=0}(r)\psi^{(v=0)}_{n,b}(R, \theta) \quad (4)$$

where $\chi_{v=0}(r)$ is the ground vibrational eigenstate of the $V^g_{H-F}(r)$ potential, and n and b are the quantum numbers associated with the vdW stretching and bending vibrations, respectively. The vdW wave function $\psi^{(v=0)}_{n,b}(R, \theta)$ is calculated variationally by diagonalizing the vibrationally averaged Hamiltonian $\hat{H}_{v,v} = \langle\chi_{v=0}(r)|\hat{H}|\chi_{v=0}(r)\rangle$ ($\hat{H}$ being the full Hamiltonian of Ar−HF), once it is represented on a suitable basis set of radial and angular functions. The vibrational diabatic approximation is fully justified here due to the large difference between the frequencies of the HF and vdW vibrations, which leads to a quite small vibrational mixing of the χ_v states.

As pointed out in the Introduction, photolysis of Ar−HF($v = 0$) is simulated starting from two different initial states of the cluster, namely, the ground vdW state (n, b) = (0, 0), and the first excited Σ bend state (n, b) = (0, 1) [this latter state being the second excited vdW state of Ar−HF($v = 0$)[29]]. The energy levels associated with these two vdW states are −101.2 and −49.0 cm^{-1} (relative to the HF($v = 0$) vibrational energy level), respectively. The angular distribution $\int dR|\psi^{(v=0)}_{n,b}(R, \theta)|^2 \sin\theta$ corresponding to each cluster initial state is displayed in Figure 1. As seen from the figure, the ground and excited vdW state distributions are concentrated mainly at low and high angles, that is, at the Ar−H−F and Ar−F−H geometries, respectively, and in this sense we speak of two cluster isomers. The two initial distributions, however, extend over the whole angular range, which means that we are dealing with large-amplitude bending motions for both cluster inital states. Related to this, we note that the distribution of the excited vdW state still has a significant amount of population in the region associated with the Ar−H−F isomeric form. The distributions of Figure 1 are qualitatively similar to the corresponding angular distributions of Ar−HBr($v = 1$),[28] except that in this latter case the distribution of the excited vdW state is more concentrated at high angles.

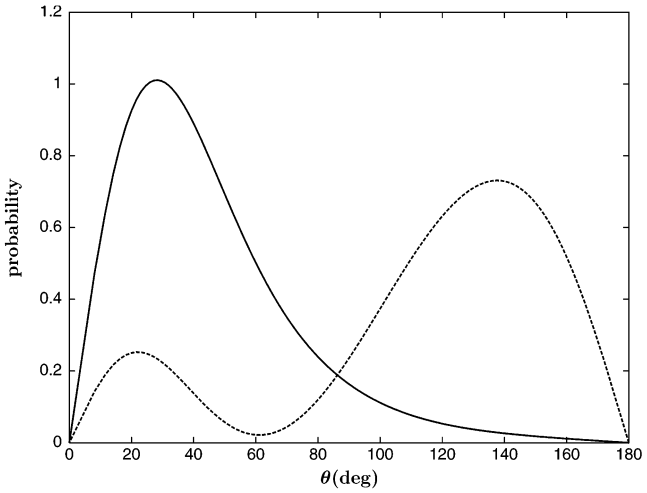

Figure 1. Angular distributions of the initial Ar−HF($v = 0$) ground (solid line) and excited (dashed line) vdW states. The distributions are normalized to unity.

B. Dynamics Simulations. Upon excitation of the cluster initial state to the upper electronic surface, the system dissociates following partial fragmentation (PF) into H + Ar−F or total fragmentation (TF) into H + Ar + F. Cluster photolysis was simulated by solving the time-dependent Schrödinger equation in the excited electronic surface, assuming zero total angular momentum ($J = 0$) for the system.

The initial cluster wave packet $\Phi_{v=0,n,b}(r, R, \theta)$ was propagated up to $t_f = 62$ fs with a time step $\Delta t = 2$ fs. At this final time, practically all the wave packet intensity has reached the asymptotic region. The Chebychev polynomial expansion method[39] was used to represent the time-evolution operator exp($-i\hat{H}\Delta t$) in the propagation scheme. The wave packet was represented on a rectangular grid of 500 × 300 equally spaced points in the r and R coordinates, respectively, in the ranges 1.0 au ≤ r ≤ 47.7 au and 5.2 au ≤ R ≤ 14.2 au. The angular coordinate was represented on a grid of 220 points corresponding to a Gauss−Legendre quadrature in the range 0° ≤ θ ≤ 180°. The Hamiltonian operations of the kinetic-energy terms involving radial coordinates were evaluated by means of fast Fourier transform techniques. The action of the angular momentum operator onto the wave packet was computed using a combination of the above angular discrete variable representation (DVR) and a finite basis representation (FBR) consisting of 150 Legendre polynomials. As we shall see below, the $A^1\Pi \leftarrow X^1\Sigma^+$ absorption spectrum of Ar−HF($v = 0$) (and therefore the wave packet) contains excitation energies remarkably higher, and in a wider range, than in the cases of Ar−HCl($v = 0$) and Ar−HBr($v = 0, 1$). This makes the present wave packet propagation a computationally more demanding problem.

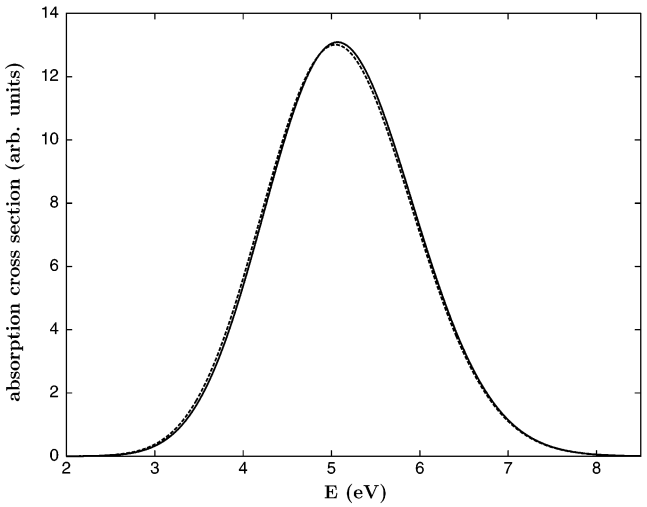

Figure 2. Absorption cross section of Ar−HF($v = 0$) from the initial ground (solid line) and excited (dashed line) vdW states of the cluster vs the excess energy E. The limit $E = 0$ corresponds to three separated atoms.

Once the time propagation was over, the fragmentation pathway yielding H + Ar−F(ν, l) products was analyzed for several excitation energies in the range of the cluster absorption spectrum. For this purpose, the asymptotic wave packet was projected out onto the product fragment states, which consist of products of a rovibrational state describing the Ar−F(ν, l) radical complex times a plane wave describing the recoiling H fragment. The projection procedure has been shown in detail elsewhere.[26a] In brief, the product fragment states are defined in the set of Jacobian coordinates associated with the Ar−F distance and the separation between H and the Ar−F center-of-mass. By means of a Jacobi transformation, these states are transformed to the (r, R, θ) coordinates in which the wave packet is represented. Then, for a given cluster excitation energy, probability amplitudes of photolysis into H and Ar−F(ν, l) products is obtained by projecting the asymptotic wave packet onto the transformed product states corresponding to that energy. The asymptotic region was considered to be $r > 20$ au, which at final time contains essentially all the wave packet.

The Ar−F radical complex supports 92 (ν, l) rovibrational states, out of which 68 are bound states with $\nu_{max} = 4$ and $l \leq 22$, and 24 are quasibound states reaching $l_{max} = 31$. The quasibound states, supported by centrifugal barriers, are very long-lived ones compared to the time scale of hydrogen dissociation, and thus they were included in the wave packet projection. The lowest bound and highest quasibound energy levels of Ar−F are 54.83 cm^{-1} below and 44.92 cm^{-1} above the dissociation limit of the Ar−F potential, respectively. Then, for each cluster excitation energy the asymptotic wave packet was projected out onto 92 degenerate states of the H and Ar−F products, for the two initial states of the parent cluster. About 20 excitation energies covering the range of the Ar−HF($v = 0$) absorption spectrum were analyzed.

III. Results and Discussion

The absorption or photodissociation cross section of Ar−HF($v = 0$) is obtained as the time to energy Fourier transform of the wave packet autocorrelation function. Figure 2 displays the cross sections corresponding to the two initial states of the cluster. The two curves are very similar since HF is the chromophore absorbing the UV photon, and the initial vibrational state of HF, $\chi_{v=0}(r)$, is the same in both cases. The different initial vdW states of the cluster only cause small differences between the two cross sections due to the weakness of the vdW interaction. Both cross sections peak about 5 eV and cover the range between 2.5 and 8 eV. This makes a difference with the absorption spectra of Ar−HCl($v = 0$)[22] and Ar−HBr($v = 0$),[30,31] which peak near 3 eV and spread from about 1.5 up to 5.5 eV, and also with the spectrum of Ar−HBr($v = 1$),[28b] that covers the range 1.3 eV $< E <$ 6 eV. The fact that the Ar−HF($v = 0$) absorption cross section is shifted to higher energies as compared to those of Ar−HCl and Ar−HBr affects greatly the fragmentation dynamics, and in particular the photolysis product yield, as we shall discuss below.

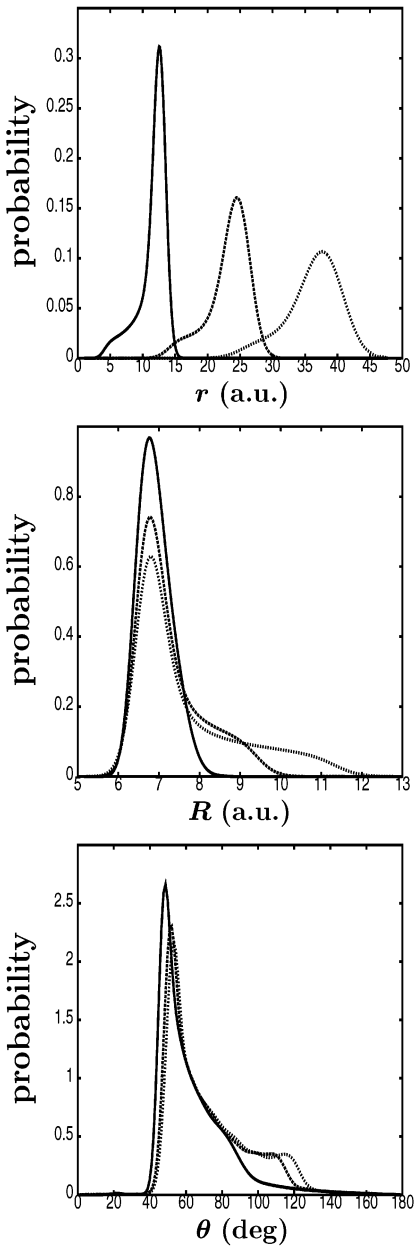

Figure 3. Wave packet probability distributions in the (r, R, θ) cluster coordinates for photolysis from the initial ground vdW state at three different times, $t = 20$ fs (solid line), $t = 40$ fs (long-dashed line), and $t = 62$ fs (short-dashed line). The angular distribution contains the sin θ factor of the volume element in Jacobian coordinates.

A. Wave Packet Dynamics. In the following, we shall analyze the Ar−HF($v = 0$) photolysis dynamics by examining the wave packet time evolution. Figure 3 shows wave packet probability distributions in the cluster coordinates at three

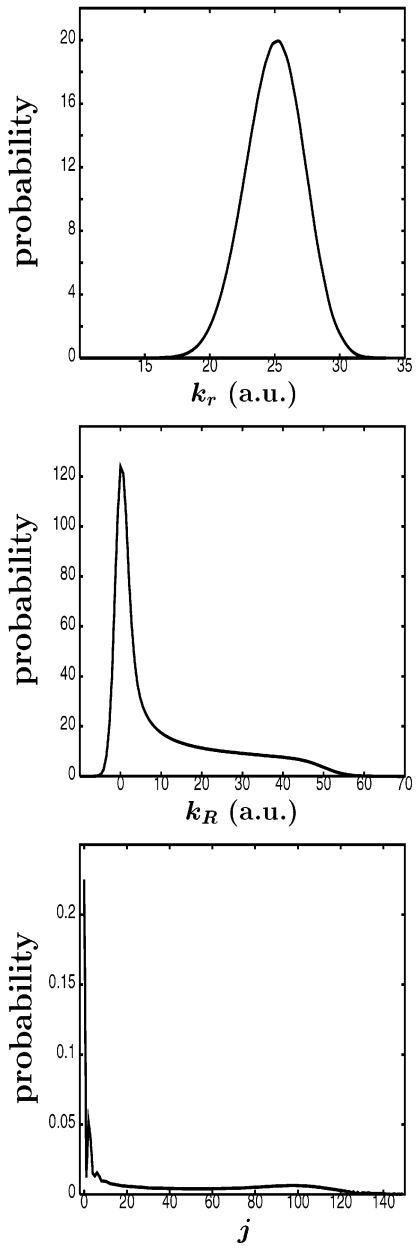

Figure 4. Wave packet probability distributions in the momenta associated with the Jacobian coordinates used in the calculations, for photolysis from the cluster initial ground vdW state at final time t = 62 fs.

different times, while Figure 4 displays probability distributions in the corresponding momenta at final time, for the initial ground vdW state of Ar−HF($v = 0$).

The main peaks of the wave packet distributions of Figure 3 show that the most likely photodissociation event is direct escaping of the hydrogen with orientations $\theta > 40°$, for which the recoiling H can overcome the Ar obstacle. In addition to the main peaks, the distributions exhibit a tail spreading toward shorter and larger distances in the cases of the r and R coordinates, respectively, and in the range $90° < \theta < 130°$ in the case of the angular distribution. Such tails in the distributions are mainly the signature of a collision between the dissociating H fragment and the Ar atom. In particular, the wave packet intensity developed at angles $90° < \theta < 130°$ (as compared with the corresponding initial distribution of Figure 1) reveals the range of final orientations at which the hydrogen is deflected after colliding with Ar. Furthermore, the small bump found near $\theta = 120°$ would be indicative of a second collision of H with the F atom, with a substantially smaller probability than the H/Ar collision. In the absence of the H/F collision, one would expect a monotonic variation of the angular intensity in the range $90° < \theta < 130°$. Good agreement is found between the present angular distribution and that obtained classically.[18]

The large intensity of the distribution tails indicates that the H/Ar collision occurs with a remarkable probability. Actually, the probability of this collision is higher in the Ar−HF($v = 0$) photolysis than in the Ar−HCl($v = 0$)[22] and Ar−HBr($v = 0$)[30,31] cases. This can be explained by invoking sterical effects related to the geometry of the initial states of the different parent clusters. In the ground vdW initial state of Ar−HF($v = 0$), the angular distribution is shifted to slightly lower θ angles than those of Ar−HCl($v = 0$) and Ar−HBr($v = 0$).[29] In addition, the initial separations between Ar and the HX center-of-mass (and thus the initial H−Ar distances) are somewhat shorter in Ar−HF($v = 0$) than in Ar−HCl($v = 0$) and Ar−HBr($v = 0$). These geometrical factors cause an increase of the probability of the H/Ar collision in the Ar−HF($v = 0$) photolysis.

The H/Ar and H/F collisions also manifest themselves in the wave packet momentum distributions of Figure 4. Indeed, the appreciable tail of the k_R distribution is indicative of energy transfer from the r mode, where the energy is initially deposited, to the R one. Such an energy transfer is also manifested in the less pronounced tail of the k_r distribution toward lower momentum values.

Interestingly, the small tail toward lower k_r momenta contrasts with the much more extending tail found in the corresponding distribution for Ar−HCl($v = 0$) photolysis.[22] Similarly, the tail of the k_R distribution of Ar−HCl($v = 0$) extended toward higher momentum values than the present one. This extensive energy transfer in the Ar−HCl($v = 0$) photodissociation was caused by multiple collisions between the hydrogen and the heavier Ar and Cl atoms.[22,27b] Thus, the shorter tails of the k_r and k_R distributions of Figure 4 indicate that only a collision between H and Ar and a subsequent, less likely H/F collision take place with appreciable probability before hydrogen dissociation. This is consistent with previous results from classical simulations of the Ar−HF($v = 0$) photolysis.[18]

The F atom has about half the mass of Cl. Besides, the excess energies deposited in the HF bond are higher (see Figure 2) than those deposited in the HCl bond of Ar−HCl($v = 0$). As a result, upon hydrogen departure the recoil velocity of F is substantially higher than that of Cl. Then, when H recoils after colliding with Ar it is likely to miss the F atom, since fluorine has travelled enough distance to avoid the collision. Since F recoils along the H−F axis, the above is particularly true for most of the initial angles, except those near the collinear configuration. For small initial orientations, the F atom recoils essentially along the R axis, and the hydrogen has the chance to encounter F after colliding with Ar. However, the weight of these initial configurations is small, which is consistent with the rather low probability of the H/F collision. This, along with the smaller size of F as compared to Cl, can explain the absence of more than two hydrogen collisions in the Ar−HF($v = 0$) photolysis.

The angular momentum distribution of the initial ground vdW state of Ar−HF($v = 0$) is very cold, with population in $j \leq 5$. Here j is the rotational quantum number corresponding to the angular momentum associated with the coordinates r and R (since $J = 0$ the angular momenta associated with the two coordinates are equal). The final wave packet j distribution of Figure 4 has the maximum at $j = 0$, two additional peaks at

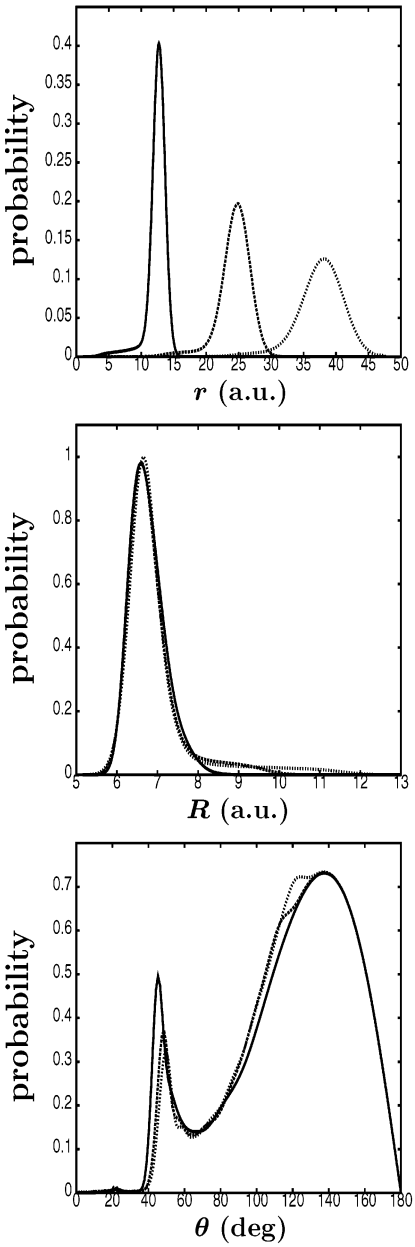

Figure 5. Same as Figure 3 for photolysis from the initial excited vdW state of Ar−HF($v = 0$).

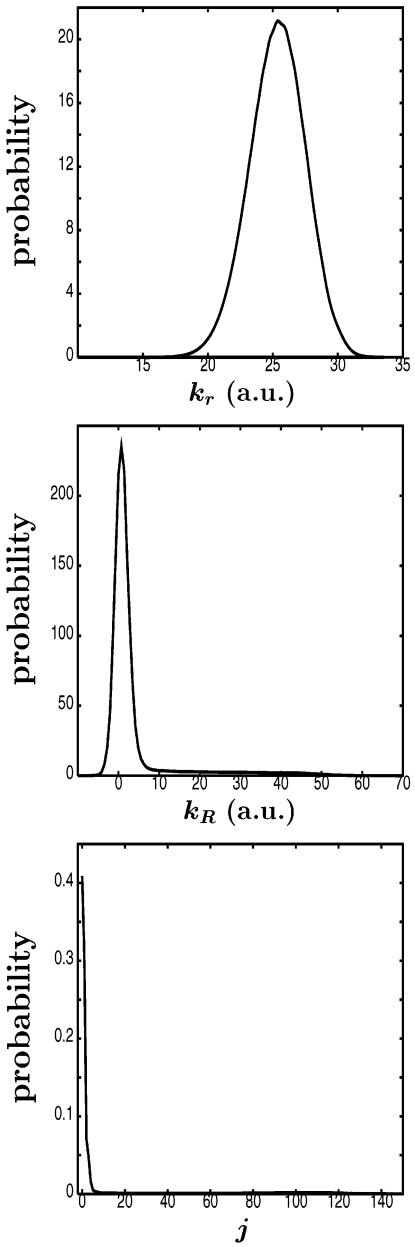

Figure 6. Same as Figure 4 for photolysis from the initial excited vdW state of Ar−HF($v = 0$).

low j, and a long tail extending up to very high angular momentum values. This distribution is similar to that obtained from Ar−HCl($v = 0$) photodissociation,[22] except that the tail at high j is more intense and reaches higher momenta in the present case. The high rotational excitation observed in the distribution is caused mainly by the H/Ar collision. The larger probability of this collision in Ar−HF($v = 0$) is consistent with the larger intensity of the distribution tail, as compared with the Ar−HCl($v = 0$) case. Due to the higher excess energies E initially deposited in Ar−HF, the hydrogen carries and therefore transfers more energy in the H/Ar collision, which explains the higher j values reached in the present distribution with respect to the Ar−HCl one.

Figures 5 and 6 show the wave packet distributions associated with Ar−HF($v = 0$) photolysis starting from the initial excited vdW state of the cluster. As seen from Figure 1, the distribution of initial hydrogen orientations in this state describes a situation where the hydrogen is mostly not hindered by the Ar obstacle. Thus, one expects that in this case the probability of the H/Ar and H/F collisions is greatly reduced with respect to photodissociation from the initial ground vdW state. Indeed, this is the result shown by the much less intense tails of the distributions of Figures 5 and 6.

All the distributions, except the angular one, are qualitatively similar to those of the initial ground vdW state, only differing in the intensity of their tails. The excited vdW state distributions are consistent with a dominantly direct hydrogen dissociation and a relatively small probability of H/Ar and H/F collisions. The collision probability is originated from the initial angular population corresponding to the Ar−H−F isomer geometries (at $\theta < 60°$, see Figure 1), much smaller than in the initial ground vdW state. This is illustrated by the wave packet angular distribution of Figure 5, which consists of two peaks originated from the two broad peaks of the initial distribution, upon essentially direct fragmentation of the hydrogen. The "shoulder" superimposed on the main peak of the distribution in the region $90° < \theta < 130°$ is the signature of the hydrogen collision events. This shoulder is similar in shape but less intense than that found

in the angular distributions of Figure 3. The angular momentum distribution of Figure 6 does not show the structure at low j values found in the corresponding distribution of Figure 4, and it only displays a weak tail toward higher j momenta. This final angular momentum distribution is actually not very different from the initial one, which is consistent with a mostly direct photodissociation dynamics.

B. Probability of Ar−F Products. The probability of the partial fragmentation pathway yielding H and Ar−F products was calculated for different excitation energies along the range of the Ar−HF($v = 0$) absorption spectrum, for the two initial cluster states. In the case of the initial ground vdW state, the probability of Ar−F radical complexes was found to be negligible (of the order of 10^{-8} in the same scale of the absorption cross section of Figure 2), for all the energies studied. The present result contrasts with previous findings (for the initial ground vdW cluster state) in the case of Ar−HCl($v = 0$) photolysis,[26] where a small but appreciable probability of Ar−Cl radicals was obtained, and in the case of Ar−HBr($v = 0, 1$) photolysis,[28,30,31] where the yield of Ar−Br products was found to be high.

As discussed elsewhere,[28b] there are essentially two factors that affect the probability of formation of Ar−X radical products upon Ar−HX photolysis. One of them is of energetic nature and is related to the amount of energy available for the Ar−X fragment (which depends on the excess energy E deposited in the HX bond and on the H/X mass ratio) and with how much of this energy can be accommodated as internal energy of Ar−X. The other factor is of dynamical nature and is related to the probability of the collision between the recoiling hydrogen and the Ar obstacle. The larger this probability, the lower the survival probability of Ar−X fragment products after cluster photolysis.

In the case of Ar−HF($v = 0$), the probability of the H/Ar collision is larger than in Ar−HCl and Ar−HBr, as discussed above, due to the geometry of the initial cluster state. Concerning the energetic factor, the excitation energies contained in the absorption spectrum of Ar−HF($v = 0$) are typically higher than in the cases of Ar−HCl($v = 0$) and Ar−HBr($v = 0, 1$), which implies higher amounts of energy available for the Ar−F fragment. Even for the same cluster excess energy E, the amount of available energy for Ar−F is larger than for Ar−Cl and Ar−Br, due to the higher H/F mass ratio as compared to the H/Cl and H/Br ones. In addition, the maximum amount of energy available which can be accommodated as internal energy of Ar−F ($\sim$100 cm^{-1}, taken as the energy of the highest Ar−F quasibound state minus the energy of the lowest Ar−F bound state) is smaller than that of Ar−Cl ($\sim$204 cm^{-1}) and Ar−Br ($\sim$225 cm^{-1}).[28] The combined effect of all these energetic and dynamical factors leads to a negligible Ar−F product yield upon photolysis from the initial ground vdW state of Ar−HF($v = 0$).

Interestingly, the probability of Ar−F formation calculated for photolysis from the initial excited vdW state of Ar−HF($v = 0$) is similarly negligible as for the ground vdW state (of the same order of magnitude, 10^{-8}), for all the energy range of the cluster absorption spectrum. Actually, the Ar−F probability for the excited vdW state is about a factor of 2−3 higher (depending on the cluster excess energy) than that for the Ar−HF($v = 0$) ground vdW state. This behavior is similar to that found for Ar−HBr($v = 1$) photolysis[28] and is the consequence of the lower H/Ar collision probability in the case of the excited vdW state, which causes a significant increase of the Ar−F product yield. Such an increase, however, is clearly insufficient in practice to raise the Ar−F yield to appreciable values.

As shown above, the main effect of the initial excited vdW state in the photolysis process is to reduce the H/Ar collision probability to a very low level. In this situation, the probability of Ar−F products is governed practically only by the energetic effects discussed above. For a given cluster excess energy E, the corresponding energy available for the Ar−F fragment distributes among center-of-mass translational energy and internal energy of Ar−F. The present result for the excited vdW state means that for all the excitation energies in the Ar−HF($v = 0$) absorption spectrum, the energy available for Ar−F is high enough such that the amount of energy going to internal energy exceeds that which can be accommodated in Ar−F without breaking. As a consequence, formation of Ar−F radical products is prevented. By extension, the same conclusion holds for photolysis from the initial ground vdW state of the cluster.

Comparison of the present findings on Ar−HF($v = 0$) photolysis with previous ones on Ar−HCl($v = 0$) and Ar−HBr($v = 0, 1$) photodissociation allows one to extract some general trends on the photolysis behavior within the Ar−HX family of clusters. As regards the probability of formation of Ar−X radical products, upon halogen substitution following the sequence F/Cl/Br, the radical yield follows the sequence zero/low/high. This sequence is governed, on one side, by the effect of the energy available for Ar−X, in the sense of decreasing the radical survival probability. This effect is extremely determinant for Ar−F and decreases substantially when going to Ar−Cl and Ar−Br, in correspondence with the decrease of the H/X mass ratio. Related to this point is the ability of the Ar−X product to accommodate this available energy as internal energy, and this ability increases from Ar−F to Ar−Br. On the other hand, for cluster initial states mainly associated with the Ar−H−X isomer geometries (e.g., the cluster ground vdW state), the radical yield is also governed by the extent to which a collision between the recoiling hydrogen and the Ar obstacle takes place. The probability of the collision depends on how much the hydrogen is initially blocked by the Ar atom. This blockage, and therefore the collision probability, decreases gradually from Ar−HF to Ar−HBr, due to geometrical factors of the cluster initial state, namely, an increase of the average hydrogen orientation and distance with respect to Ar. As the effect of the energy available for Ar−X decreases significantly (as in the case of Ar−HBr), the effect of the H/Ar collision plays a more important role in determining the Ar−X probability. This can be exploited to increase the Ar−X product yield, since the collisional effect can be largely reduced by starting the cluster photolysis from an excited vdW state associated with Ar−X−H isomer geometries. Photolysis of the Ar−HI precursor cluster (not studied theoretically so far) is expected to follow the trends outlined above.

Experiments on UV photolysis of the $(HI)_2$ and $(HCl)_2$ clusters[3,4] have found evidence of formation of I−HI and Cl−HCl radical products, respectively. Photolysis of Ar−HX (or in general Rg−HX) and $(HX)_2$ clusters has some common features as far as the formation of Rg−X or X−HX radical products is concerned. Indeed, for both types of parent clusters hydrogen dissociation must be direct, to avoid a collision with the Rg or HX obstacle, and then the yield of formation of Rg−X or X−HX products is essentially governed by the energy available for them. The main difference is that the X−HX radicals are more strongly bound than their isoelectronic Rg−X counterparts, which increases their ability to accommodate the available energy as internal energy, and therefore their survival probability. In this sense, the present results for Ar−HF($v = 0$) photodissociation can be extrapolated in order to make a

qualitative prediction about the yield of possible F−HF products upon photolysis of $(HF)_2$. On the basis of the dramatic effect of the energy available for the radical found in this work, we expect the F−HF yield to be rather low. This extrapolation should be, of course, taken with caution.

IV. Conclusions

The ultraviolet photolysis dynamics of the Ar−HF($v = 0$) cluster is investigated through wave packet simulations. In the simulations, photolysis starts from two different cluster initial states, namely, the ground vdW state, associated with Ar−H−F isomer geometries, and an excited vdW bending state, associated with Ar−F−H isomer geometries. The wave packet dynamics for the initial ground vdW state shows a cluster fragmentation where the hydrogen dissociates mainly in a direct way, and at most a collision with the Ar atom and a subsequent, less likely collision with F take place. The H/Ar collision is found to be more likely than in the photolysis of Ar−HCl($v = 0$) and Ar−HBr($v = 0, 1$), starting also from the cluster ground vdW state. Such a result is due to the fact that hydrogen dissociation is somewhat more hindered by the Ar obstacle in the case of the Ar−HF($v = 0$) initial state. Despite the higher probability of the first H/Ar collision, the probability of a second hydrogen collision with F is rather low, and no appreciable evidence of further collisions is found, as was the case in Ar−HCl and Ar−HBr photodissociation. The absence of more than two hydrogen collisions is attributed to the fast recoil of the F atom, which lowers substantially the probability of an encounter with hydrogen after the first H/Ar collision. Cluster photolysis from the initial excited vdW state is dominated by direct hydrogen dissociation events to a larger extent than in the case of the ground vdW state. Only a rather small probability of a H/Ar collision is found, as a consequence of the initial distribution of intracluster orientations associated with the excited vdW state.

The yield of Ar−F photolysis products has been calculated for different excitation energies covering the range of the Ar−HF($v = 0$) absorption spectrum, for the two initial states of the cluster. A negligible probability of Ar−F products is found in the whole energy range for both initial states. It is concluded that the energy available for the Ar−F fragment is too high as to allow survival of this radical complex. Finally, by comparison of the present results for Ar−HF($v = 0$) to previous ones on Ar−HCl and Ar−HBr UV photodissociation, some general trends are outlined on the photolysis behavior and formation of Ar−X radical products within the family of Ar−HX precursor clusters.

Acknowledgment. This work was supported by C.I.C.Y.T. (Ministerio de Ciencia y Tegnología), Spain, Grant No. BFM-2001-2179, and by the European network TMR, Grant No. HPRN-CT-1999-00005.

References and Notes

(1) Segall, J.; Wen, Y.; Singer, R.; Wittig, C.; García-Vela, A.; Gerber, R. B. *Chem. Phys. Lett.* **1993**, *207*, 504.

(2) Jaques, C.; Valachovic, L.; Ionov, S.; Wen, Y.; Böhmer, E.; Segall, J.; Wittig, C. *J. Chem. Soc., Faraday Trans.* **1993**, *89*, 1419.

(3) Zhang, J.; Dulligan, M.; Segall, J.; Wen, Y.; Wittig, C. *J. Phys. Chem.* **1995**, *99*, 13680.

(4) Liu, K.; Kolessov, A.; Partin, J. W.; Bezel, I.; Wittig, C. *Chem. Phys. Lett.* **1999**, *299*, 374.

(5) Young, M. A. *J. Chem. Phys.* **1995**, *102*, 7925.

(6) Plusquellic, D. F.; Votava, O.; Nesbitt, D. J. *J. Chem. Phys.* **1994**, *101*, 6356.

(7) Votava, O.; Plusquellic, D. F.; Myers, T. L.; Nesbitt, D. J. *J. Chem. Phys.* **2000**, *112*, 7449.

(8) Mackenzie, S. R.; Votava, O.; Fair, J. R.; Nesbitt, D. J. *J. Chem. Phys.* **1996**, *105*, 11360; **1999**, *110*, 5149.

(9) Baumfalk, R.; Buck, U.; Frischkorn, C.; Gandhi, S. R.; Lauenstein, C. *Chem. Phys. Lett.* **1997**, *269*, 321.

(10) Baumfalk, R.; Buck, U.; Frischkorn, C.; Nahler, N. H.; Hüwel, L. *J. Chem. Phys.* **1999**, *111*, 2595.

(11) Baumfalk, R.; Nahler, N. H.; Buck, U.; Niv, M. Y.; Gerber, R. B. *J. Chem. Phys.* **2000**, *113*, 329.

(12) Slavíček, P.; Žďánská, P.; Jungwirth, P.; Baumfalk, R.; Buck, U. *J. Phys. Chem. A* **2000**, *104*, 7793.

(13) Picconatto, C. A.; Ni, H.; Srivastava, A.; Valentini, J. J. *J. Chem. Phys.* **2001**, *114*, 7073.

(14) Alimi, R.; Gerber, R. B. *Phys. Rev. Lett.* **1990**, *64*, 1453.

(15) García-Vela, A.; Gerber, R. B.; Imre, D. G.; Valentini, J. J. *Phys. Rev. Lett.* **1993**, *71*, 931.

(16) García-Vela, A.; Gerber, R. B.; Buck, U. *J. Phys. Chem.* **1994**, *98*, 3518.

(17) Schröder, T.; Schinke, R.; Mandziuk, M.; Bačić, Z. *J. Chem. Phys.* **1994**, *100*, 7239. Schröder, T.; Schinke, R.; Bačić, Z. *Chem. Phys. Lett.* **1995**, *235*, 316.

(18) Schröder, T.; Schinke, R.; Liu, S.; Bačić, Z.; Moskowitz, J. W. *J. Chem. Phys.* **1995**, *103*, 9228.

(19) Christoffel, K. M.; Bowman, J. M. *J. Chem. Phys.* **1996**, *104*, 8348.

(20) Narevicius, E.; Moiseyev, N. *Chem. Phys. Lett.* **1998**, *287*, 250; *Mol. Phys.* **1998**, *94*, 897.

(21) Monnerville, M.; Pouilly, B. *Chem. Phys. Lett.* **1998**, *294*, 473.

(22) García-Vela, A. *J. Chem. Phys.* **1998**, *108*, 5755.

(23) Niv, M. Y.; Krylov, A. I.; Gerber, R. B.; Buck, U. *J. Chem. Phys.* **1999**, *110*, 11047.

(24) Žďánská, P.; Schmidt, B.; Jungwirth, P. *J. Chem. Phys.* **1999**, *110*, 6246. Žďánská, P.; Slavíček, P.; Jungwirth, P. *J. Chem. Phys.* **2000**, *112*, 10761.

(25) Schmidt, B. *Chem. Phys. Lett.* **1999**, *301*, 207.

(26) (a) Juanes-Marcos, J. C.; García-Vela, A. *J. Chem. Phys.* **2000**, *112*, 4983. (b) Juanes-Marcos, J. C.; García-Vela, A. *J. Chem. Phys.* **2001**, *115*, 5692 (E).

(27) (a) Juanes-Marcos, J. C.; García-Vela, A. *J. Phys. Chem. A* **2002**, *106*, 236. (b) Juanes-Marcos, J. C.; García-Vela, A. *J. Phys. Chem. A* **2002**, *106*, 5445.

(28) (a) Prosmiti, R.; García-Vela, A. *J. Chem. Phys.* **2002**, *117*, 100. (b) Prosmiti, R.; García-Vela, A. *J. Chem. Phys.* **2003**, *118*, 8268.

(29) Prosmiti, R.; García-Vela, A. *Chem. Phys. Lett.* **2002**, *366*, 238.

(30) Lepetit, B.; Lemoine, D. *J. Chem. Phys.* **2002**, *117*, 8676.

(31) Trin, J.; Monnerville, M.; Pouilly, B.; Meyer, H.-D. *J. Chem. Phys.* **2003**, *118*, 600.

(32) Auer, B. M.; McCoy, A. B. *J. Phys. Chem. A* **2003**, *107*, 4.

(33) Špirko, V.; Piecuch, P.; Bludský, O. *J. Chem. Phys.* **2000**, *112*, 189.

(34) Hutson, J. M. *J. Chem. Phys.* **1992**, *96*, 6752.

(35) Dunning, T. H. *J. Chem. Phys.* **1976**, *65*, 3854.

(36) Tang, K. T.; Toennies, J. P. *Chem. Phys.* **1991**, *156*, 413.

(37) Aquilanti, V.; Luzzati, E.; Pirani, F.; Volpi, G. G. *J. Chem. Phys.* **1988**, *89*, 6165.

(38) Beswick, J. A.; Jortner, J. *Adv. Chem. Phys.* **1981**, *47*, 363.

(39) Tal-Ezer, H.; Kosloff, R. *J. Chem. Phys.* **1984**, *81*, 3967.